



Contents

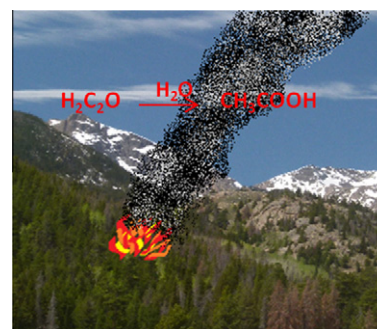
EDITOR'S CHOICE

1-4

Acetic acid formation via the hydration of gas-phase ketene under ambient conditions

Tara F. Kahan, Thomas K. Ormond, G. Barney Ellison, Veronica Vaida

Research highlights ► The hydration of gas-phase ketene was monitored using infrared spectroscopy. ► Acetic acid, acetic acid dimer, and acetic anhydride were observed at 295 K. ► This reaction is proposed as a source of acetic acid in biomass burning plumes.



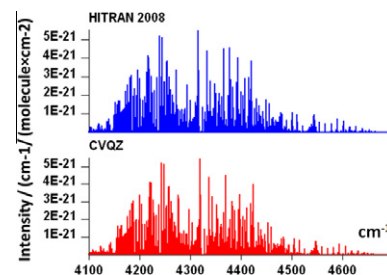
GASEOUS MOLECULES

5-11

New dipole moment surfaces of methane

Andrei V. Nikitin, Michael Rey, Vladimir G. Tyuterev

Research highlights ► New *ab initio* dipole moment surfaces of methane were constructed. ► Integrated intensities for seven lower polyads up to $J = 30$ were calculated. ► Symmetry property of dipole moment surfaces of methane was considered. ► The fourth order DMS was found not sufficient for 5-vibration-quanta bands.

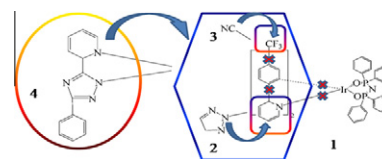


12-17

Theoretical study of injection, transport, absorption and phosphorescence properties of a series of heteroleptic iridium(III) complexes in OLEDs

Xiaohong Shang, Deming Han, Dongfeng Li, Zhijian Wu

Research highlights ► The charge transfer properties are affected by the cyclometalated ligands. ► The designed complex **4** possesses best hole and electron transfer abilities. ► The designed complex **4** is a potential candidate for blue phosphorescent material.

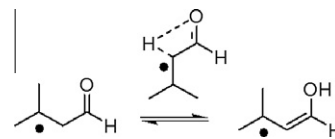


18–21

The failure of UMP2 on the keto–enol tautomerization of β -radical compounds: The effect of spin contamination

Yu-Wei Huang, Venkatesan Srinivasadesikan, Wei-Hong Chen, Shyi-Long Lee

Research highlights ► We examine the relative stability of α -, β - and γ -ketonic and enolic radicals. ► In α - and γ -radicals, UMP2 and DFT schemes all favor ketonic form. ► In β -radicals, the UMP2 favors ketonic radical. ► In β -radicals, DFT and CCSD(T) schemes prefer enolic ones. ► The failure of UMP2 comes from the spin contamination problem for enolic form.

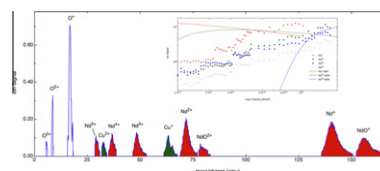


22–27

Strong-field ionization and Coulomb explosion of small neodymium and europium oxide clusters

Matt W. Ross, A.W. Castleman Jr.

Research highlights ► Ultraintense laser pulses used to probe the ionization properties. ► High charges of europium and neodymium measured using ISS. ► Ionization of 4f electrons are explored. ► Metal–oxygen bond strength governs the overall cluster ionization behavior.

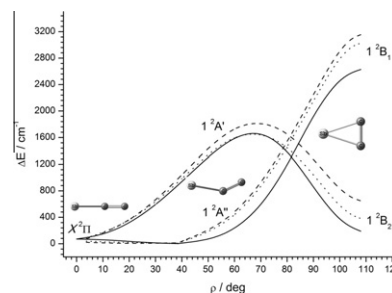


28–34

An *ab initio* study of antimony dicarbide (C_2Sb)

Milan Z. Milovanović, Stanka V. Jerosimić

Research highlights ► Characterization of a new molecular species: C_2Sb . ► High-level *ab initio* calculation including spin–orbit effects. ► The molecule is found to be quasi-linear. Three relevant geometries are reported. ► Dissociation energy is found to be relatively large. ► The low-lying excited valence-type electronic states description is given.



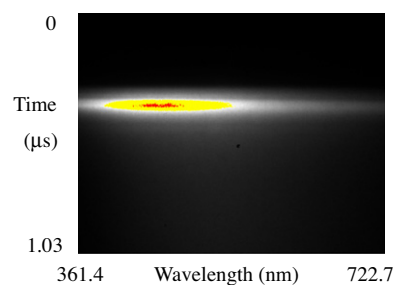
CONDENSED PHASES

35–39

Radiation of light from powder materials under shock compression

Takamichi Kobayashi

Research highlights ► Intense and broad radiation of light was observed when powder materials were shock compressed. ► The radiation of light was observed even for very weak shocks. ► Thermal radiation of shock-compressed powder material is unlikely the source of the radiation. ► Adiabatically-compressed residual gas in powder appears responsible for the radiation of light.

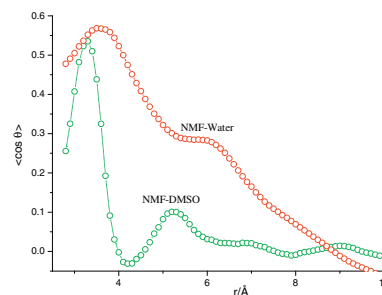


40–44

Hydrogen bonding donation of *N*-methylformamide with dimethylsulfoxide and water

Alexandre Borges, João M.M. Cordeiro

Research highlights ► Hydrogen bonding of NMF with DMSO and water has been investigated. ► The NMF–DMSO hydrogen bond is significantly shorter and stronger than the NMF–water. ► The NMF–solvent dimers are much more stable in the NMF–DMSO mixture. ► The DMSO molecules dislocate the molecules of water bonded to the amine hydrogen.

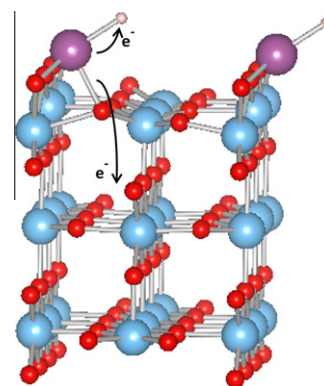


45–51

Support effect on H adsorption on a metal atom

Zeineb Helali, Alexis Markovits, Christian Minot, Manef Abderrabba

Research highlights ► We examine the support effect of a TiO_2 surface on H adsorption on a metal atom ($M=\text{K}$ to Zn). ► For $M=\text{K}$, Co , Ni and Cu , the TiO_2 support yields a decrease of M–H interactions strength. ► For $M=\text{Ca}$ to Fe and for Zn , the TiO_2 support increases the strength of M–H interaction. ► Increase occurs when M possesses two or more easily transferable electrons.

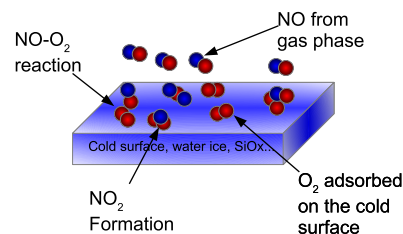


52–55

Formation of nitrogen oxides via $\text{NO} + \text{O}_2$ gas–solid reaction on cold surfaces

M. Minissale, E. Congiu, S. Baouche, H. Chaabouni, A. Moudens, F. Dulieu, G. Manicó, V. Pirronello

Research highlights ► We unveil that O_2 adsorbed on a cold surface reacts with a very high efficiency with NO . ► NO_2 is formed independently of the surface composition and morphology. ► The oxidation of NO has implications for the complex atmospheric chemistry of Antarctica. ► The reaction $\text{NO} + \text{O}_2$ is of fundamental importance to understand of the full $\text{NO} + \text{O}_x$ reaction scheme in astrophysics.

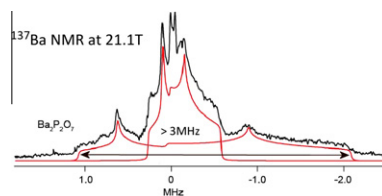


56–60

A combined ultra-wideline solid-state NMR and DFT study of ^{137}Ba electric field gradient tensors in barium compounds

Luke A. O'Dell, Igor L. Moudrakovski

Research highlights ► Ultra-wideline ^{137}Ba solid-state NMR obtained from five Ba-containing materials with highly asymmetric barium environments. ► The WURST-QCPMG sequence and magnetic field of 21.1 T greatly reduce experimental time. ► One of two resolved sites in $\alpha\text{-Ba}_2\text{P}_2\text{O}_7$ shows a C_Q of 42.3 ± 0.3 MHz, the largest obtained for ^{137}Ba in a powder. ► The experimental quadrupolar parameters are in excellent agreement with the DFT calculations.

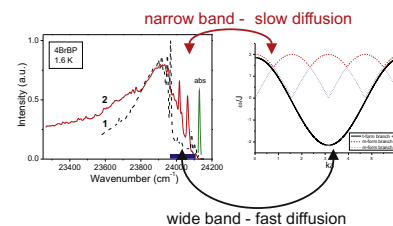


61–64

Low-temperature phosphorescence and triplet exciton transport in 4-bromobenzophenone polymorphs

M.A. Strzhemechny, D.I. Zloba, O.S. Pyshkin, L.M. Buravtseva

Research highlights ► Phosphorescence spectra of two polymorphs of 4-bromobenzophenone were measured at 1.6 K. ► The differences in the spectra are ascribed to differences in triplet exciton diffusivities. ► Within a 1D model based on crystal structures exciton bands were calculated for both forms. ► Phosphorescence data corroborate the inference that diffusion in the triclinic form is faster.



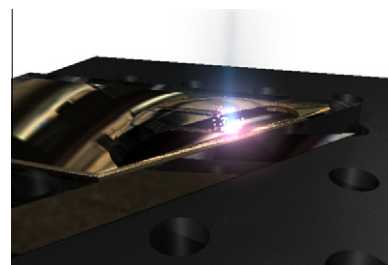
NANOSTRUCTURES AND MATERIALS

65–68

Size control of gold nanoparticles produced by laser ablation of thin films in an aqueous environment

D.M. Bubb, S.M. O'Malley, Jonathan Schoeffling, Richard Jimenez, Brian Zinderman, SunYong Yi

Research highlights ► Au nanoparticles were formed by laser ablation of thin films with a liquid drop placed on top. ► The size can be controlled by the thickness of the film. ► A simple calculation shows that the temperature in the vicinity of the ablation crater strongly influences the nucleation rate and the size of the particles.

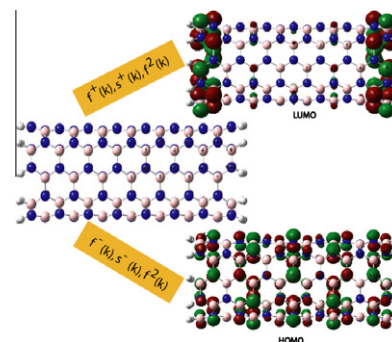


69–73

DFT-based reactivity study of (5,5) armchair boron nitride nanotube (BNNT)

Soumen Saha, Tandabany C. Dinadayalane, Danuta Leszczynska, Jerzy Leszczynski

Research highlights ► MPA and NBO analyses are used to calculate DFT-based local reactivity descriptors. ► We have identified favorable sites for the electrophilic and nucleophilic attacks on the armchair (5,5) BNNT with open edges. ► Observed reactivity trends are in agreement with the electron density distributions of the molecular orbitals of BNNT.

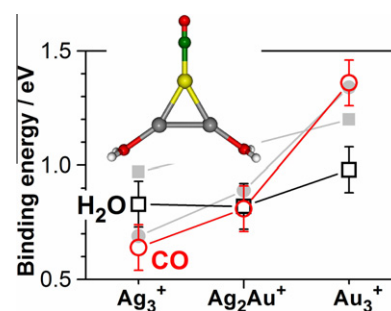


74–79

Composition dependent selectivity in the coadsorption of H₂O and CO on pure and binary silver–gold clusters

Irene Fleischer, Denisia M. Popolan, Marjan Krstić, Vlasta Bonačić-Koutecký, Thorsten M. Bernhardt

Research highlights ► Composition dependent reactivity of mass-selected Ag_nAu_m⁺ clusters has been investigated. ► Binding energies of H₂O to Ag_nAu_m⁺ (n + m = 3) have been determined experimentally and theoretically. ► Coadsorption of CO and H₂O to Ag_nAu_m⁺ has been observed only for Ag₂Au⁺. ► First step for a catalytic water gas shift chemistry on Ag_nAu_m⁺ has been established.



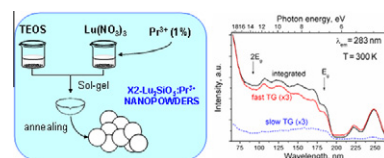
80–85

Structural characterisation and time-resolved luminescence spectroscopy of nanocrystalline $X_2\text{-Lu}_2\text{SiO}_5\text{:Pr}^{3+}$ powders

M. Trevisani, K.V. Ivanovskikh, N. Grillet, F. Piccinelli, M. Bettinelli

Research highlights ► Nanopowders of $X_2\text{-Lu}_2\text{SiO}_5\text{:Pr}^{3+}$ were prepared by the sol–gel route.

- The nanoparticles have revealed an oval shape with average dimensions of 35×44 nm.
- Efficient and fast energy transfer from host to the Pr^{3+} 5d states was observed.
- Short Pr^{3+} 5d–4f decay times were observed upon both direct and band-gap excitation.
- A significant temperature dependence of the decay times was evidenced, different from the corresponding single crystal.

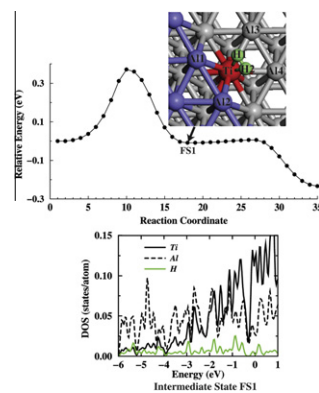


86–91

Surface step enhanced H_2 splitting on Ti-doped Al(1 1 1) surface

Mengmeng Zheng, Gang Chen

Research highlights ► The doping of Ti in surface step region can gain ~ 0.36 eV higher doping energy. ► Activation energy is reduced to as low as 0.45 eV for aluminum hydrogenation. ► Ti doped in the lowest energy structure could remain as recycling active catalyst. ► H_2 in intermediate state gains 0.3 e charge due to Kubas interaction mechanism.

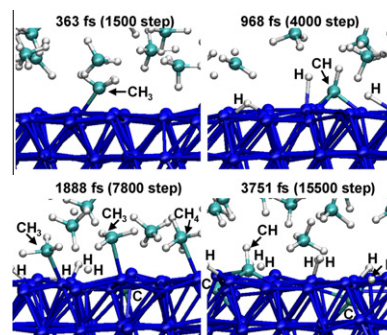


92–97

Ab initio molecular dynamics simulation of dissociation of methane on nickel(1 1 1) surface: Unravelling initial stage of graphene growth via a CVD technique

Yasushi Shibuta, Rizal Arifin, Kohei Shimamura, Tomoya Oguri, Fuyuki Shimojo, Shu Yamaguchi

Research highlights ► Dissociation of methane on $\text{Ni}(111)$ surface is examined by *ab initio* MD simulation. ► Methane on Ni surface is dissociated into isolated atoms via CH_3 and CH fragments. ► Carbon atoms are buried into the subsurface of nickel layers after the dissociation.

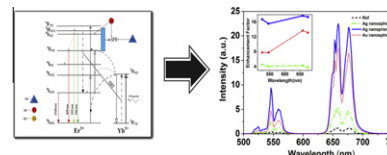


98–101

Enhancement of luminescent emission in $\text{Er}^{3+}/\text{Yb}^{3+}$ co-doped $\text{Y}_2\text{Ti}_2\text{O}_7$ films with Ag/Au nanoparticles

Yanling Liu, Feng Song, Jiadong Liu, Jun Zhang, Yin Yu, Hongyan Zhao

Research highlights ► The enhanced luminescences were demonstrated with silver/gold nanoparticles doping. ► The strong enhanced near infrared emission were observed. ► More intense upconversion emission bands were observed. ► Two mechanisms explained the reasons of the above enhanced emissions.



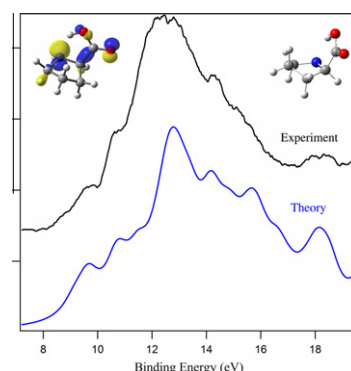
BIOMOLECULES

102–107

Valence ionization of L-proline amino acid: Experimental and theoretical study

F. Fathi, H. Farrokhpour

Research highlights ► The valence photoelectron spectrum of L-proline is reported. ► Theoretical methods were used to confirm the experimental spectrum. ► Natural bonding orbital calculation was also used to assign the ionization bands. ► Theory and experiment are in good agreement.

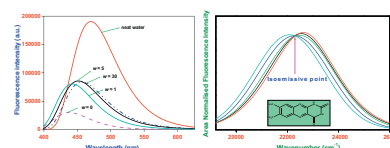


108–115

Effect of nano-confinement on the photophysics of lumichrome

Banibrata Maity, Aninda Chatterjee, Debabrata Seth

Research highlights ► The photophysics of lumichrome was studied in reverse micelles. ► In EG and glycerol reverse micelle τ_{rot} value increases with w value. ► An isoemissive point in TRANES was observed in reverse micelle.

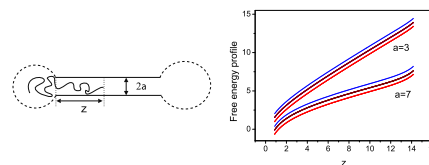


116–121

A theoretical study on entropy-driven polymer translocation through a finite-sized nanochannel

Fanlong Meng, Ming Li, Xin Zhou, Zhongcan Ouyang

Research highlights ► We theoretically study polymer translocation through finite-length nanochannels. ► The position of polymer leading end is applied as reaction coordinate. ► The free energy of polymer is a linear function of the reaction coordinate. ► The entropy driven force is insensitive to most of system parameters. ► The theoretical results are helpful in understanding recent experiments.



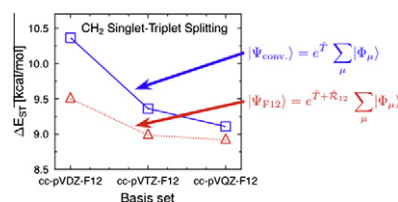
NEW EXPERIMENTAL OR THEORETICAL METHODS

122–127

Explicitly correlated internally contracted multireference coupled-cluster singles and doubles theory: ic-MRCCSD(F12*)

Wenlan Liu, Matthias Hanauer, Andreas Köhn

Research highlights ► We propose an explicitly correlated internally contracted multireference coupled-cluster method, ic-MRCCSD(F12*). ► The F12 geminal contributions strongly improve the basis set convergence of the correlation energy. ► The extra computational cost in comparison to the parent method, ic-MRCCSD, is small. ► The ic-MRCCSD(F12*)+(T) method produces very accurate results, even in combination with minimal active spaces.

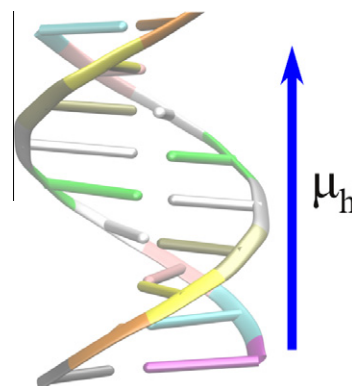


128–131

Hole mobilities of periodic models of DNA double helices in the nucleosomes at different temperatures

Attila Bende, Ferenc Bogár, János Ladik

Research highlights ▶ HF band structures of poly(G–C) and poly(A–T) with sugar-phosphate are presented. ▶ The hole mobilities were determined using the deformation potential approximation. ▶ The mobilities increase with decreasing temperatures.

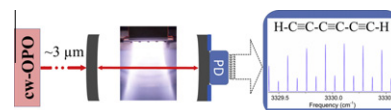


132–137

Mid-infrared continuous wave cavity ring-down spectroscopy of a pulsed hydrocarbon plasma

Dongfeng Zhao, Joseph Guss, Anton J. Walsh, Harold Linnartz

Research highlights ▶ A flexible OPO-based cw-CRDS spectrometer. ▶ A hardware based multi-trigger concept to apply cw-CRDS to pulsed sample systems. ▶ High-resolution infrared spectroscopy of hydrocarbon chains.

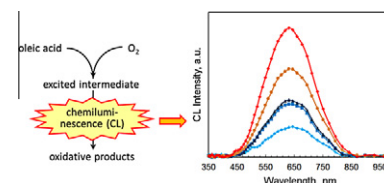


138–142

Analysis of chemiluminescence spectra in oxidative degradation of oleic acid

Tomohiro Sago, Hiroshi Ishii, Hideaki Hagihara, Noriyuki Takada, Hiroyuki Suda

Research highlights ▶ The thermal oxidation of oleic acid was investigated using chemiluminescence (CL). ▶ The CL spectra included peaks for singlet oxygen and excited carbonyls. ▶ The structures of oxidative product were determined by IR and NMR. ▶ The emission peaks were suggested to shift as a result of the structure.

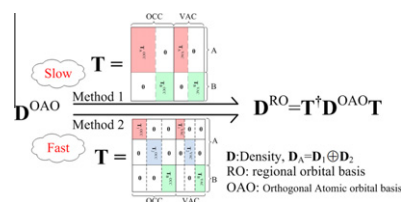


143–147

A modified localization scheme for the three-dimensional elongation method applied to large systems

Kai Liu, Yun-an Yan, Feng Long Gu, Yuriko Aoki

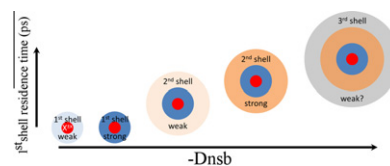
Research highlights ▶ A modified localization scheme for three dimensional elongation method to the large system calculations is proposed. ▶ The modified localization scheme is based on the small dimensional elongation units. ▶ The modified scheme is more efficient than the original one. ▶ The accuracy of the new scheme is the same as original one.



148–150**Ion solvation structure and dynamical information via deviations from the solvent-berg diffusion model**

Stuart A. Bogatko

Research highlights ► We decompose the ion diffusion into solvent-berg and non-solvent-berg components. ► The non-solvent-berg component has 2 distinct regimes. ► For many cations the non-solvent-berg component is proportional to 1st shell residence time. ► The 1st shell residence time serves as a proxy for an ion's structure building ability.



The Publisher encourages the submission of articles in electronic form thus saving time and avoiding rekeying errors. Please refer to the online version of the Guide for Authors at <http://www.elsevier.com/locate/cplett>

SciVerse ScienceDirectFull text of this journal is available, on-line from **ScienceDirect**. Visit www.sciencedirect.com for more information.